*Am J Physiol Cell Physiol* 284: C934–C943, 2003.
First published December 11, 2002; 10.1152/ajpcell.00234.2002.

# Mechanical loading: biphasic osteocyte survival and targeting of osteoclasts for bone destruction in rat cortical bone

**Brendon S. Noble,[1,2] Nicky Peet,[3] Hazel Y. Stevens,[1,2] Alex Brabbs,[3] John R. Mosley,[1] Gwendolen C. Reilly,[3] Jonathan Reeve,[2] Timothy M. Skerry,[3] and Lance E. Lanyon[1]**

[1]*Department of Veterinary Basic Science, Royal Veterinary College, London NW1 0TU;*
[2]*University Department of Medicine, Addenbrooke's Hospital, Cambridge CB2 2QQ;*
*and* [3]*Department of Biology, University of York, York YO10 5YW, United Kingdom*

Submitted 21 May 2002; accepted in final form 30 September 2002

**Noble, Brendon S., Nicky Peet, Hazel Y. Stevens, Alex Brabbs, John R. Mosley, Gwendolen C. Reilly, Jonathan Reeve, Timothy M. Skerry, and Lance E. Lanyon.** Mechanical loading: biphasic osteocyte survival and targeting of osteoclasts for bone destruction in rat cortical bone. *Am J Physiol Cell Physiol* 284: C934–C943, 2003. First published December 11, 2002; 10.1152/ajpcell.00234.2002.—Bone is removed or replaced in defined locations by targeting osteoclasts and osteoblasts in response to its local history of mechanical loading. There is increasing evidence that osteocytes modulate this targeting by their apoptosis, which is associated with locally increased bone resorption. To investigate the role of osteocytes in the control of loading-related modeling or remodeling, we studied the effects on osteocyte viability of short periods of mechanical loading applied to the ulnae of rats. Loading, which produced peak compressive strains of −0.003 or −0.004, was associated with a 78% reduction in the resorption surface at the midshaft. The same loading regimen resulted in a 40% relative reduction in osteocyte apoptosis at the same site 3 days after loading compared with the contralateral side ($P = 0.01$). The proportion of osteocytes that were apoptotic was inversely related to the estimated local strain ($P < 0.02$). In contrast, a single short period of loading resulting in strains of −0.008 engendered both tissue microdamage and subsequent bone remodeling and was associated with an eightfold increase in the proportion of apoptotic osteocytes ($P = 0.02$) at 7 days. This increase in osteocyte apoptosis was transient and preceded both intracortical remodeling and death of half of the osteocytes ($P < 0.01$). The data suggest that osteocytes might use their U-shaped survival response to strain as a mechanism to influence bone remodeling. We hypothesize that this relationship reflects a causal mechanism by which osteocyte apoptosis regulates bone's structural architecture.

in vivo; rat ulnae; osteocytes; cell death

TO MAINTAIN STRENGTH, the vertebrate skeleton needs to adapt to the prevailing mechanical needs of the organism (46). Part of this adaptation involves adding new bone in regions that require it. In a complementary way, there is targeted sculpting of each bone internally and externally to remove redundant or mechanically incompetent (5) bone tissue. The effector cells for this process are the osteoclasts, which share the early part of their lineage with monocyte/macrophages. How cells are precisely targeted to where resorption is needed is poorly understood.

The osteogenic effects of loading and of load engendered strains have been evident for some time (4, 9, 22), but it has not been clear which cell type or types may be responsible for sensing load and for targeting effector cell activity in vivo. Osteocytes are considered to be likely candidates for this role because of their distribution throughout the bone matrix, their ability to respond to strain with biochemical signals such as nitric oxide and prostaglandins (23, 39, 45), and their existence as part of a syncytial network comprising osteocytes, osteoblasts, bone lining cells, endocytes lining the vascular sinusoids of bone, and perhaps also sympathetic nerve fibers associated with bone's vascular supply. However, with few exceptions (23, 39), it has not been previously possible to identify osteocyte-specific behavior at a microscopic level that is related spatially to the strain environment and is associated with localized remodeling activity.

Mechanical loads influence the morphology and hence the function of many other tissues in the body. Loading provides a directional influence to cells during development, aiding pattern formation, and also in part controls the life and death cycle of cells directly involved with the resistance to mechanical forces in other tissues (7, 12, 15). The mechanisms by which mechanical forces elicit these cellular responses are incompletely understood. In some cell types tension influences the viability of cells, leading directly to changes in the shape of soft tissues through cell loss (6). Understanding mechanical influence on tissue shaping and turnover will play a fundamental role in our ability to treat a number of age-related disease states and to engineer tissues for transplantation.

Loading is known to be an important factor in the formation and maintenance of skeletal architecture. Bone morphology adapts to suit functional loading

Address for reprint requests and other correspondence: B. S. Noble, Musculo-Skeletal Research Unit, The Univ. of Edinburgh Medical School, Level 3, Pathology Area, Teviot Place, Edinburgh EH8 9AG, UK (E-mail: Brendon.Noble@ed.ac.uk).

The costs of publication of this article were defrayed in part by the payment of page charges. The article must therefore be hereby marked "*advertisement*" in accordance with 18 U.S.C. Section 1734 solely to indicate this fact.

patterns by responding to the size and distribution of strains that loading engenders in the bone tissue (8, 21, 22, 46). This involves modifying locally the rates of bone formation and resorption. The osteocyte is a former osteoblast that has become embedded in the bone matrix. It communicates with other osteocytes and with cells at the bone surface via gap junctions on filamentous cell projections that pass through canaliculi in the bone matrix. While the osteocyte population responds to increased loading by producing a number of molecules thought to be involved in osteogenesis (17, 20, 27, 34, 36), osteocytes can also undergo apoptotic cell death if they lie in bone tissue that is undergoing rapid remodeling (2, 31).

We previously proposed that the marked apoptosis of osteocytes observed in women and in female rats subjected to acute estrogen withdrawal provides a targeting mechanism for inducing the well-documented removal of bone by osteoclasts and hence could be important in understanding the pathogenesis of postmenopausal and other forms of osteoporosis (32, 40, 41). This was because, apart from the effects on function of losing active osteocytes, in general, apoptotic cells profoundly influence the behavior of those cells that reside in close proximity to them. They are rapidly phagocytosed by both migrating cells of the monocyte/macrophage lineage or nonprofessional phagocytic cells and influence gene expression and cytokine release (48, 49). The alternative possibility was that the observed apoptosis of osteocytes was induced by signals or function-related activity originating from the newly arrived osteoclasts. If this were true, osteocyte apoptosis might be merely an epi-phenomenon associated with the remodeling process. Determining whether osteocyte apoptosis could be an important initiating mechanism for bone resorption required an acute experiment to determine whether it occurs widely before the arrival of osteoclasts within bone experimentally targeted for resorption.

Here we investigated the effect of using applied mechanical strain to both switch on and switch off targeted bone resorption and the apoptotic death of osteocytes in regions of cortical bone. Controlled mechanical loads were applied that were known to be sufficient to either suppress local bone resorption and replace it with bone formation (30) or promote physical microdamage to the bone matrix, leading to vigorous remodeling of the damaged bone (1, 5, 29). In this second group of experiments, we have taken advantage of the finite time interval between inducing damage and the local appearance of osteoclasts to determine whether the apoptosis of osteocytes might precede or succeed the appearance of the osteoclasts that begin the process of removing and replacing the damaged bone.

## METHODS

### *Ulna Loading Regimes*

*Physiological loading experiment.* The rat ulna-loading model used in this study has been reported previously and used to demonstrate strain-magnitude-related changes in modeling activity (13, 30). All animal procedures were approved by the ethics committee of the host institution and were conducted under the authority of a United Kingdom Government Home Office Licence. Sprague-Dawley rats were purchased with a body weight range of 180–190 g 1 wk before the start of loading and housed in pairs throughout the experimental period. After the induction of general anesthesia, the left antebrachium was held in padded cups between the olecranon process of the ulna and the flexed carpus and was subjected to controlled dynamic axial loading as previously described (13, 30). Between anesthetic periods, normal cage activity was allowed.

Loads were applied daily on *days 1–5* and *8–12* inclusive. The loading waveform was trapezoid, and the load necessary to produce the required peak strain magnitude at the ulna midshaft was determined from strain-gauged specimens (30). In the higher physiological strain group ($n = 6$), the peak strain at the ulna midshaft was $-0.004$ (i.e., $-4{,}000$ microstrain), and in the lower physiological strain group, it was $-0.003$ ($n = 3$; medium strain group). Applied and released strain rates were 0.035 $s^{-1}$. On each day the loaded bones were subject to 1,200 loading cycles at a frequency of 2 Hz.

*Supraphysiological loading experiment.* Nonrecovery pilot experiments were performed to determine the loading regimen that would engender microdamage without producing gross fracture. As in previous studies, loading was applied at 2 Hz but the peak strain and number of cycles were altered. These pilot experiments showed that a reliable indicator of microdamage occurred when the forearm was shortened in length by 1.5 mm. At peak strains of $-0.008$, plastic (nonrecoverable) deformation usually occurred within $<1{,}000$ cycles. Further loading after the 1.5-mm shortening invariably caused fracture within 10 additional cycles. For the supraphysiological strain experiments, we therefore used a peak strain of $-0.008$ and used forearm shortening as the indicator of comparable levels of microdamage, despite the disadvantage that different animals received different numbers of loading cycles (normally from 15 to 50).

After recovery following supraphysiological loading, there were no fractures in any animals, and limb use appeared normal on recovery from anesthesia. Thirty male Sprague-Dawley rats ($\sim$100 g body mass, age 7–8 wk) were used in the supraphysiological loading studies. The bones from six animals were collected immediately after the end of loading and used for bulk fluorescein staining followed by confocal microscopy. Bones from two groups of four animals euthanized 7 and 14 days after the end of loading were used for cryosectioning for DNA, tartrate-resistant acid phosphatase (TRAP), lactate dehydrogenase (LDH), and apoptosis assessment. The bones of a further six animals were collected, two each at 7, 14, or 28 days after loading, for plastic embedding and confocal microscopy.

The animals received three labels of calcein (Sigma, Poole, UK) to label bone forming surfaces by intraperitoneal injection (at a dose of 10 mg/kg) 7, 5, and 3 days before loading and then 2, 4, 7, 9, 11, 14, 16, 18, 21, 23, and 25 days after loading (if they were not previously killed).

After the end of loading the animals were killed at the previously specified times by an overdose of barbiturate, and the bones were variously processed according to the analysis that was to be performed. To confirm the effect of overloading on the accumulation of microdamage in bones, ulnae from overloaded animals were dissected and bulk stained in a water-soluble sodium salt of fluorescein (Sigma) dissolved in Ringer's solution. To achieve a flat surface for confocal microscopy, the periosteum and a small amount of subperios-

teal bone were removed by gentle polishing at the central regions of the medial and lateral surfaces with fine-grade carborundum paper and then with 0.5-μm alumina paste. The bones were then examined intact with a Bio-Rad DVC 250 confocal microscope, using a × 60 oil objective.

*Preparation of Cryostat Sections*

The left (loaded) and right (normal) forelimbs were removed and dissected of some soft tissue, leaving muscle and periosteum intact, and their length was measured from the proximal olecranon to the lateral styloid process. The midshaft and 3 mm on either side were marked on the bone for reference to enable sampling at a functionally equivalent site in the pairs of normal and loaded bones. The bones were immediately coated in 5% polyvinyl alcohol, snap-frozen in a hexane chilling bath, and stored at −70°C until use. Cryostat sections (8 μm thick) prepared from bone samples were mounted perpendicularly on chucks with the distal end uppermost after being trimmed down to 3 mm from the midshaft. Serial cross sections were taken throughout the midshaft zone so that the point 80 μm distal to the exact midshaft could be located. The osteoblastic response to loading was measured by first capturing fluorescent images of fixed material from control and loaded bones from each animal on a low light level camera and then measuring the separation between periosteal calcein labels. Complete absence of surface labels on a crenellated surface indicated local resorption. Sections were collected from each level investigated and stored fresh at −20°C (for osteocyte LDH determination) or 4°C for TRAP, or they were fixed in 4% formaldehyde in phosphate-buffered saline (PBS) and stored at 4°C (for DNA labeling).

*In Situ Identification of Osteocyte DNA Fragmentation Using Nick Translation*

Briefly, fragmented DNA was detected in cell nuclei in situ using a previously described method (31) in which the sensitivity of the system has been reduced to increase specificity for cells containing large numbers of DNA breaks. Sections were fixed in 4% formaldehyde for 10 min, washed three times in PBS, and air-dried before demineralization in 0.25 mol/l EDTA in 50 mmol/l Tris·HCl, pH 7.4, for 10 min. One group of sections was treated with DNase (0.2 mg/ml PBS; Sigma) for 1 h (positive control) to produce breaks in the DNA. Sections were then treated with nick translation mixture, which consisted of 3 μmol/l digoxygenin (DIG)-11-dUTP, 3 μmol/l each of dGTP, dATP, and dCTP, 50 mmol/l Tris·HCl, pH 7.5, 5 mmol/l $MgCl_2$, and 0.1 mmol/l dithiothreitol, either with or without (negative control) 0.5 U/100 μl Kornberg polymerase for 1 h at 37°C (all reagents obtained from Roche Diagnostics). Sections were washed in PBS and incubated with fluorescein isothiocyanate (FITC)-labeled anti-DIG antibody and 5% normal sheep serum in PBS for 1 h at room temperature. After being washed, sections were counterstained for nuclear DNA with propidium iodide (Sigma), mounted in Citifluor (Agar Scientific, Stansted, UK), and examined by fluorescence microscopy. Digital images were collected for image analysis.

*DNA Gel Electrophoresis*

For extraction of DNA, 20 further sections were collected from each bone. With the use of fine forceps, the bone component of each section was removed for analysis, excluding most of the marrow cells and tissue external to the cortex. In this way samples for DNA extraction were enriched for osteocytes (31). DNA was extracted from 20 undecalcified cryostat sections per ulna (each 10 μm thick) using a Nucleon DNA extraction kit (Scotlab, Glasgow, UK) (31). After extraction, DNA was precipitated in ethanol and pelleted. To retrieve any small DNA fragments from the supernatant, it was also treated with 0.2 mol/l sodium acetate at −20°C for 24 h and spun to a pellet. Both pellets were then combined and solubilized in Tris-borate-EDTA-loading buffer before ~10 μg of DNA were run on a 1.5% agarose gel at 20 V for 16 h. For reference, a 100-bp standard was included. DNA was visualized under ultraviolet light after incubation of the gel in ethidium bromide.

*Assessment of Long-Term Cell Viability In Situ by LDH Activity*

Cells that were viable at the time of sampling were identified in unfixed 8-μm-thick cryostat sections by means of their LDH activity. Histochemical staining was performed according to published methods (47) with minor modifications (31). LDH-positive cells were visualized by light microscopy. LDH-positive cells in six fields per section (×400 magnification; area = 0.074 $mm^2$) were counted and expressed as the number of positive cells per field.

*Localization of Bone Formation and Resorption Activity in Resin-Embedded Bone*

Groups of animals killed at 7, 14, and 28 days, respectively, after loading were used for assessment of long-term changes in cortical remodeling activity after induction of microdamage. Briefly, bones to be assessed for remodeling activity were fixed in increasing concentrations of ethanol and then placed in LR white resin for 5 days before polymerization overnight at 60°C. Using a Leitz low-speed saw, we cut 100-μm sections from regions of each bone that spanned the zone in which the analysis of osteocyte apoptosis was made in cryostat sections.

*Mapping of Apoptotic Osteocytes in Ulnar Cross Sections*

Mapping of apoptotic osteocytes was approached in two ways. Maps of cross sections showing cells treated by nick translation and counterstained with propidium iodide to show nuclear DNA were constructed by piecing together low-power (×100) micrographs. The analysis was performed on a Macintosh computer by using the public domain NIH Image program (developed at the National Institutes of Health and available at http://rsb.info.nih.gov/nih-image/). Osteocytes were then counted according to their distribution in predetermined zones based on anticipated strains (see below). Finally, individual osteocytes were mapped by their positive or negative distance from the horizontally orientated neutral strain axis and categorized according to whether they stained for DNA breaks.

Radial distribution data were generated by dividing the cross section into 11 boxed areas radiating from the center of mass. Starting from a fixed point on the bone perimeter (defined as the farthest point from the center of mass on the cranial aspect), the number of total osteocytes staining positive for propidium iodide was calculated for each area. Similarly, the density of apoptotic cells (FITC positive) was calculated for the same zones and ratios of apoptotic to total cells calculated.

The captured images were used to map the exact location of individual osteocytes so that the anticipated strain experienced by individual cells could be calculated, using strain data published previously (42). The positions of the apoptotic

cells were each marked on the map, and the distance of each osteocyte (apoptotic or nonapoptotic) from the neutral strain axis was determined. The strain maps derived from previous work (42) were superimposed on these maps of the cortical cross sections so that the strain value irrespective of sign experienced by each osteocyte could be estimated. Histograms were then constructed of the proportions of apoptotic osteocytes identified within incremental "bins," each of which spanned a range of 300 microstrain. This was to permit an evaluation of the statistical effect of calculated strain on osteocyte apoptosis in the experimentally loaded and nonloaded ulnae. The density of apoptotic osteocytes in each "bin" was calculated from the density of total osteocytes in the relevant regions multiplied by the proportion that stained positive for DNA breaks.

### *Age of Osteocytes and Their Propensity to Undergo Apoptosis*

To determine whether the change in the rate of production of new osteocytes brought about by loading might explain the decreased incidence of apoptosis, we categorized the age of osteocytes by pulse-labeling the bone with fluorescent mineralization markers (as described above). Osteocytes could, therefore, be categorized as born before or after the dates of fluorochrome administration. The calcein labels delineated regions of bone that were less or greater than 10 days old.

### *Statistical Analysis*

Results are reported as means ± SE for six animals unless otherwise stated and were compared using a nonparametric matched-pair Wilcoxon signed rank test of loaded vs. control contralateral limb. Results were considered significantly different at $P < 0.05$ (2-tailed test).

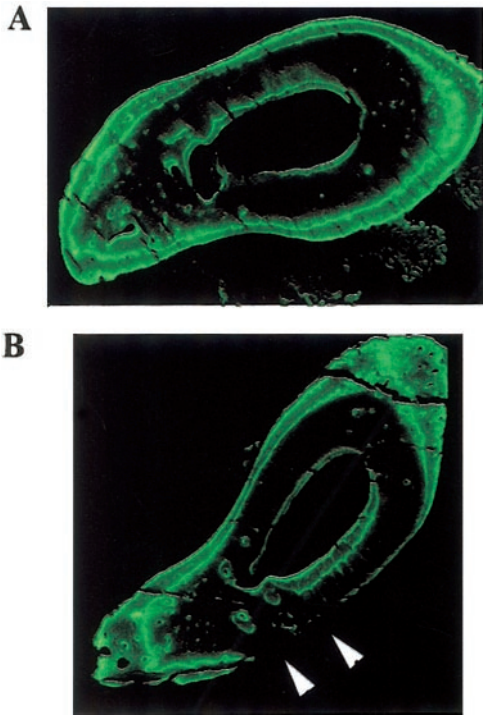


Fig. 1. *A*: cross section of bone showing calcein labeling (green/yellow) typical of adaptive osteogenic response seen in ulna loaded to −0.004 microstrain. *B*: cross section of contralateral control ulna showing resorption surface (with no calcein labeling) on its perimeter (arrowheads).

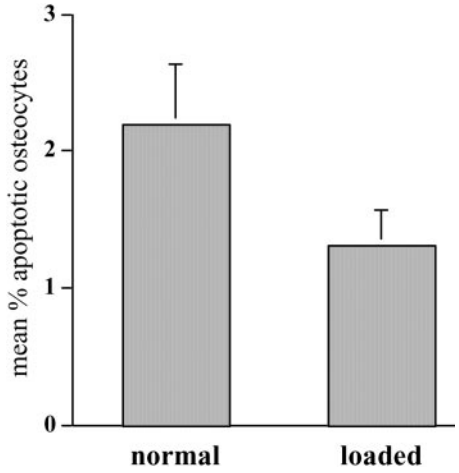


Fig. 2. Percentages of osteocytes showing highly fragmented DNA for 6 animals comparing loaded with normally exercised contralateral ulnae. The number of osteocytes in the entire bone cross section was determined by combining maps of propidium iodide-stained sections. Values are means ± SE.

## RESULTS

### *Loading to Produce Physiological Levels of Strain*

*Modeling activity after bone loading.* Axial loading of one forelimb of each rat to a peak strain magnitude of −0.004 (−4,000 microstrain) for 10 min each day for 10 days produced an osteogenic antiresorptive response as reported in previous studies (13, 30). In the loaded limb, instead of the resorptive activity seen on the medial surface at the midshaft region of the control ulnae, there was bone formation as evidenced by calcein labels (Fig. 1, *A* and *B*). The relative extent of the resorption surfaces was reduced by 78 ± 22.1% ($P < 0.02$), and the formation surface length increased in relative terms by +14 ± 4.0% ($P < 0.02$). Axial loading of forelimbs to a peak strain magnitude of −0.003 for 10 min each day for 10 days produced an increase in formation surface length (+19.3 ± 7.4%) similar to that seen in the −0.004 strain group. The reduction in resorption surface (−59 ± 15.9%) was not as marked as in the −0.004 strain group, but the difference between groups was not significant (Student's $t = 1.4$ NS).

*Osteocyte apoptosis.* The proportion of osteocytes displaying a signal for fragmented DNA was determined at identical positions along the length of the bone cortex in loaded and control limbs. The percentage of apoptotic osteocytes was reduced in loaded compared with control limbs in both the high −0.004 strain group (41.67 ± 7.08% reduction, $n = 6$, $P < 0.01$) and the −0.003 strain group (30.13 ± 5.39% reduction, $n = 3$).

When the data from the −0.004 and −0.003 groups were combined, average values for the percentage of apoptotic osteocytes in the control and loaded limbs were 2.20 ± 0.43 and 1.32 ± 0.25%, respectively ($n = 9$ for difference, $P = 0.017$) (see also Fig. 2). In these groups, there was a nonsignificant correlation between

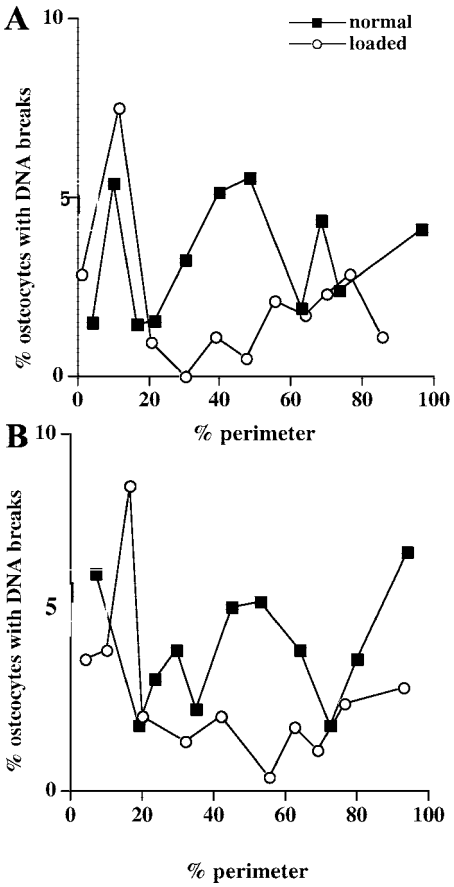


Fig. 3. Radial distribution of percentages of osteocytes affected by apoptosis in the radii of 2 individual rats (*A* and *B*). Osteocytes were plotted radially around the cortex in 11 zones of equal perimeter length. Normally loaded control ulnae are contrasted with loaded ulnae. Note the similarity in the distribution of apoptosis in control limbs and the loss of a large area affected by apoptosis after loading.

the extent of decrease in proportion of apoptosis and the extent of decrease in the length of resorption surface ($r = +0.56$).

The radial distribution of cortical osteocytes at the midshaft of the control limb loaded only by the animals' everyday activity demonstrated a number of spatially defined peaks of apoptotic activity. In the loaded limb the major peak of apoptotic cells found in the cortical bone adjacent to the resorption surface was almost completely or completely abolished, as in the two examples shown (Fig. 3).

*Osteocyte apoptosis and strain magnitude.* When osteocytes were mapped in relation to their position in the local strain environment, we found that regions of relatively high physiological levels of strain magnitude contained low numbers of apoptotic cells, whereas regions experiencing low peak strain magnitudes had higher numbers of apoptotic osteocytes. Hence, there was a linear relationship between the reciprocal of peak strain magnitude and the number per area ($r = 0.78$) ($P = 0.02$ with 6 degrees of freedom) (Fig. 4) and the proportion of apoptotic osteocytes in the cortex ($P = 0.06$; data not shown) with a pronounced increase in the probability of encountering an apoptotic osteocyte as the neutral strain axis was approached.

*Age of osteocytes and their propensity to undergo apoptosis.* The loading regime increased the amount of more recently formed bone (as evidenced by distance between the calcein labels) and, hence, the number of "younger" osteocytes. The density of apoptotic osteocytes resident in mineralized matrix that had been laid down for <10 days (expressed as the percentage of osteocytes with highly fragmented DNA) was similar to that for osteocytes >10 days old (old: 3.46 ± 1.01%; new: 3.73 ± 0.90%; $P = 0.84$).

### *Damage-Inducing Levels of Loading*

*Identification of microdamage induction.* Confocal microscopy confirmed that, immediately after loading to a peak strain of −0.008, there was clear evidence of cortical bone matrix microdamage in the form of numerous fluorescein-labeled cracks ~5 μm long and 1 μm or less wide. Cross-hatched cracks characteristic of compressive forces were seen on the concave/medial side of the bone that is loaded in compression as a result of axial loading of the ulna (13), whereas diffuse damage typical of tensile forces was seen on the convex side of the bone that is loaded in tension as a result of its position on the outer longitudinally convex surface of the ulna (42). Damage was most dense in the midshaft, where the strains induced by loading were highest, because the bending moment is greatest here, becoming less dense proximal and distal to this (13).

*Damage-inducing loads and osteocyte apoptosis.* Seven days after loading there was a highly significant increase in the proportion of apoptotic osteocytes in

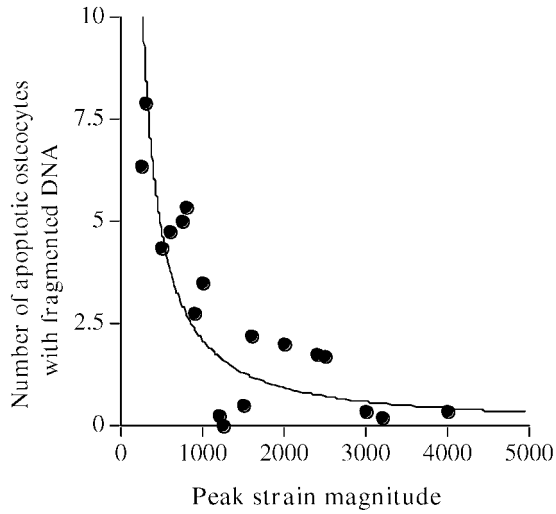


Fig. 4. Relationship between peak strain magnitude and the density of apoptotic osteocytes in the cortex of physiologically loaded bones. The density of apoptotic osteocytes is expressed per mm$^2$. Rat ulnar cortices were loaded to −4,000 or −3,000 microstrain, and load experienced by each cell was estimated from strain maps (see text). Cells with similar strain experience irrespective of sign were grouped into strain-range "bins," and the density of apoptotic cells was calculated from the density of total osteocytes staining positive for DNA breaks within each bin ($r = 0.78$; $P = 0.02$ with 6 degrees of freedom for physiological loading experiment).

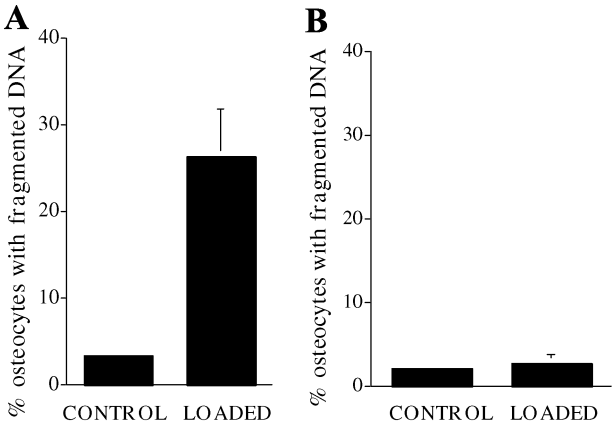


Fig. 5. Percentage of osteocytes displaying evidence of DNA fragmentation in bones experiencing normal and damage-inducing levels of load. Sections of rat ulnae from normally loaded (control) and overloaded limbs 7 and 14 days after the loading stimulus are shown. *A*: 7 days after loading. *B*: 14 days after loading. Values are mean percentages (±SD) of total osteocytes showing DNA fragmentation.

−0.008 strain bones (26.3 ± 5.4 vs. 3.3 ± 0.2%, $n = 4$, $P = 0.02$), compared with contralateral control ulnae in the same animals (Fig. 5*A*). Apoptotic cells were distributed throughout the cortex of the overloaded bones (Fig. 6*B*), whereas in control bones the distribution of apoptotic cells was more sparse (Fig. 6*A*). Labeling for fragmented DNA was accompanied by large-scale disintegration of the nucleus as shown under high-power light microscopy (Fig. 6*C*). At this time (7 days), there was no evidence of intracortical remodeling, as demonstrated by a complete absence of intracortical resorption spaces or TRAP activity (data not shown).

In sections taken 14 days after loading, there were fewer osteocytes with fragmented DNA in the loaded bones than there had been in sections taken 7 days after loading so that, at 14 days, there was no significant difference between loaded and control bones (2.74 ± 1.06 vs. 2.06 ± 0.59%, $n = 4$, $P = 0.67$) (Fig. 5*B*).

DNA ladders were clearly apparent in samples extracted from loaded (Fig. 7, *lanes 2* and *3*) but were less intense in contralateral control bones 7 days after commencement of the experimental loading protocol (*lane 5*). Fourteen days after loading, these ladders were of much reduced intensity (*lane 6*) and resembled the control contralateral samples.

*Live and dead cells (LDH activity).* At 7 days after loading, when many cells were showing signs of DNA damage, there was no difference in the numbers of LDH-positive cells in loaded bones (26.58 ± 1.45 cells/field, $n = 4$) compared with control bones (25.08 ± 1.08, $n = 4$, $P = 0.64$). However, by 14 days after the end of loading, the number of viable cells was decreased in loaded bones by ~50% (12.22 ± 0.96 vs. 29.56 ± 1.35, $n = 4$, $P < 0.01$).

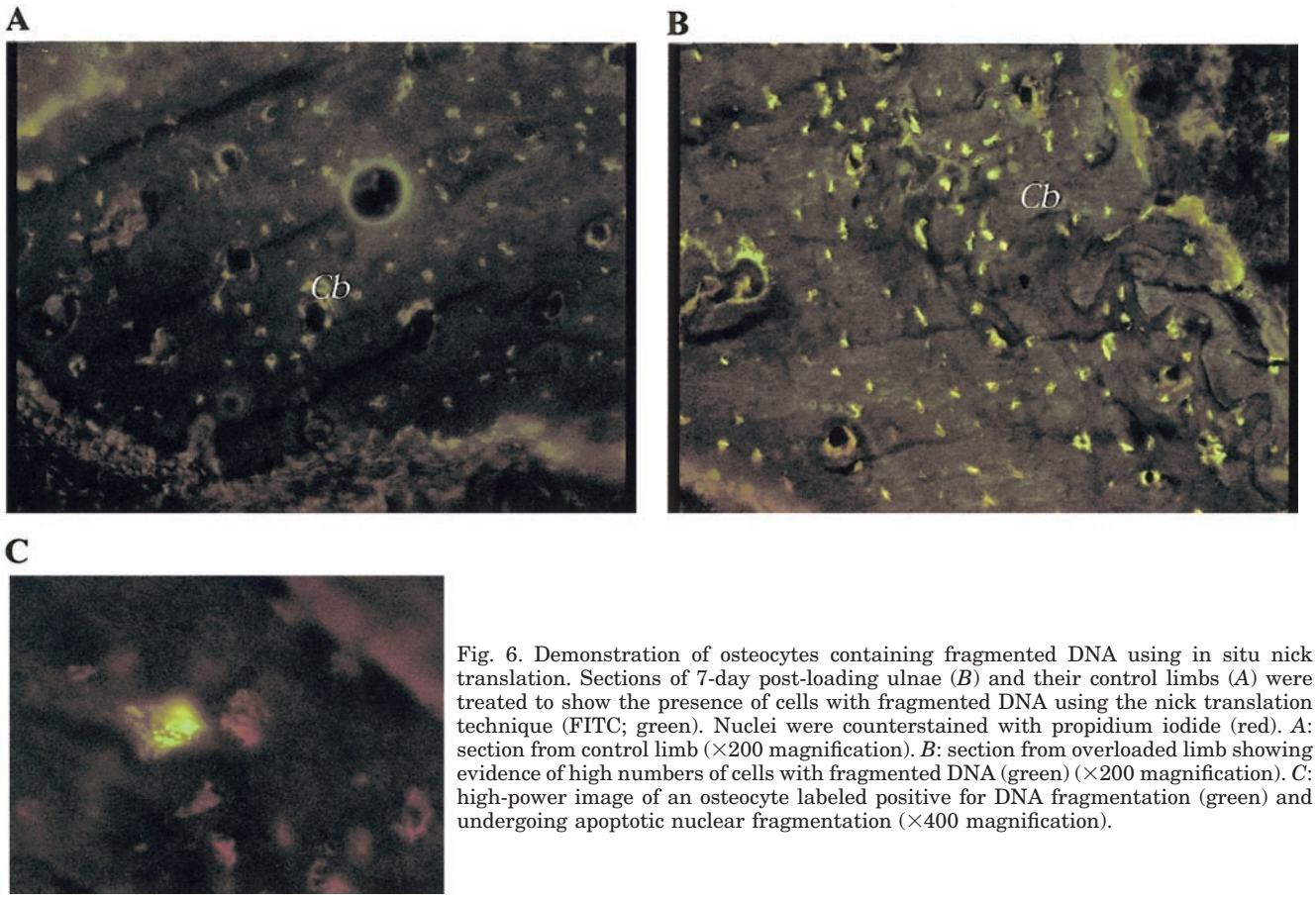


Fig. 6. Demonstration of osteocytes containing fragmented DNA using in situ nick translation. Sections of 7-day post-loading ulnae (*B*) and their control limbs (*A*) were treated to show the presence of cells with fragmented DNA using the nick translation technique (FITC; green). Nuclei were counterstained with propidium iodide (red). *A*: section from control limb (×200 magnification). *B*: section from overloaded limb showing evidence of high numbers of cells with fragmented DNA (green) (×200 magnification). *C*: high-power image of an osteocyte labeled positive for DNA fragmentation (green) and undergoing apoptotic nuclear fragmentation (×400 magnification).

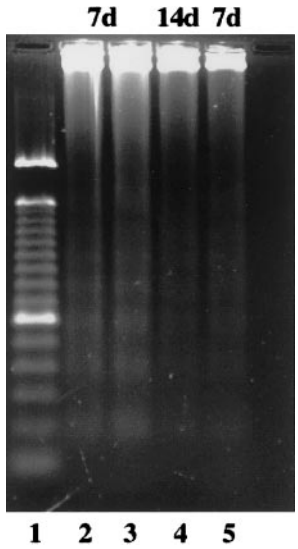


Fig. 7. Agarose gel electrophoresis of DNA extracted from cryostat sections of ulnae at 7 and 14 days (d) after overloading. *Lane 1*: standard 100-bp DNA markers. *Lanes 2* and *3*: DNA extracted from bone 7 days after overloading shows evidence of fragments ~180 bp apart (DNA laddering), indicative of apoptosis. *Lane 4*: 7-day control limb showing reduced evidence of DNA ladders. *Lane 5*: DNA extracted from bone 14 days after overloading. *Lane 6*: empty.

*Intracortical remodeling activity after overloading.* Seven days after induction of microdamage, minimal evidence of intracortical remodeling was seen in the control or treated ulnae, which showed clear uninterrupted fluorescent labels representing previous periosteal and endosteal bone formation throughout the cortex. After 14 days, evidence of osteoclastic resorption was seen in the cortices as demonstrated by the transection of previously incorporated labels by new Haversian canals showing crenellated edges (Fig. 8). Intracortical resorption activity was absent in the cortices of control ulnae. Twenty-eight days after loading, infilling of resorption spaces was evident from incorporation of fluorochrome labels, as demonstrated by concentric infilling of defects that transected previous lamellar bone incorporating labels.

## DISCUSSION

We have shown that mechanical loading has the capacity to regulate apoptosis in osteocytes. Loading to produce strains within the physiological range appeared to reduce apoptosis, but loading at damagingly high levels increased apoptosis. Therefore, there appeared to be a U-shaped relationship between osteocyte survival and the strain they experienced. As expected, the damage engendered by high loading was followed by intracortical remodeling.

### *Effects of Nondamaging Mechanical Loading*

The prevalence of osteocyte apoptosis is reduced after short durations of mechanical loading inducing peak dynamic strains of −0.003 or −0.004. These loading regimens induced adaptive rather than reparative responses characterized by appositional bone formation on previously resorbing surfaces and increased bone formation on surfaces already undergoing formation (13, 30). Our data demonstrate that these load-induced changes in growth-related bone modeling are accompanied by a reduction in the normal, distinct spatial pattern of osteocyte apoptosis evident in the nonloaded ulnar cortex (Fig. 3). The region exhibiting the major concentration of apoptotic osteocytes in control bones was adjacent to resorbing bone surfaces (13, 30). Similar regions of apoptotic activity have been described in other tissues undergoing growth-related modeling and remodeling changes (6).

The loading regimen engendering peak strains of −0.004 reduced resorption and also osteocyte apoptosis to a greater extent than the regimen producing peak

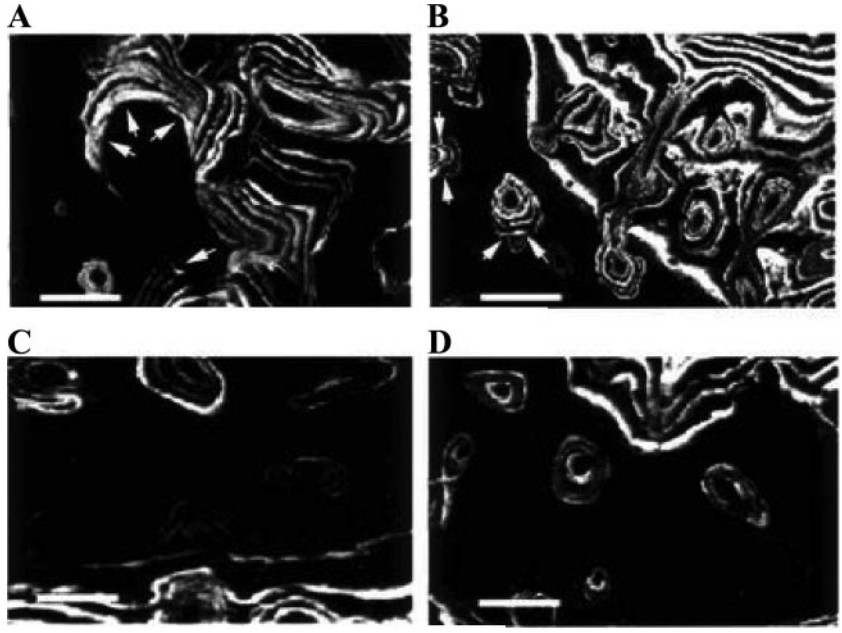


Fig. 8. Secondary remodeling in rat ulna after a single episode of loading 2 or 4 wk previously. *A*: 14-day overloaded bone showing large lacunae with resorption of previously labeled concentric lamellae (arrows). *B*: 28-day overloaded bone with mature Haversian systems showing infilling of resorption lacunae that cut through previously labeled lamellae of a primary osteon (arrows). *C*: 14- and 28-day control bones showing primary osteons with calcein-labeled concentric lamellae. Scale bars = 100 μm.

strains of −0.003. Because the other important variables of the loading (frequency, mode, and rate) were identical, it is likely that there is some form of dose dependence between the incidence of apoptosis and the peak strain magnitude. Whether these other loading variables such as rate, mode, and frequency have the ability to influence osteocyte apoptosis is outside the scope of our present study.

An inverse relationship was found between osteocyte apoptosis and the calculated strain magnitudes experienced by the osteocytes, which were estimated from direct measurements in previous experiments. Although these calculations (42) had some limitations, which have been discussed elsewhere (30), they support the concept that nondamaging strain promotes osteocyte viability. This might be due to the effects of strain on intracellular antiapoptotic pathways (see below) or because the nutrition or oxygen supply of the osteocytes is enhanced by the effects of strain on intracanalicular fluid flow (10, 25).

*Effect of Damage-Inducing Mechanical Loading*

In the experiments where peak strain was −0.008, damage was induced immediately by loading followed in a clear sequence by osteocyte apoptosis and intracortical remodeling. We know from previous studies that the loading regimen used resulted in a deterioration of the material properties of the bone (1), and we used shortening as a surrogate for that deterioration because we found that it predicted with great accuracy the point at which loading would be followed by overt fracture within 10 cycles.

Intracortical remodeling is not a frequent feature of rat bone, although it has been shown to occur in some circumstances including secondary hyperparathyroidism and prostaglandin treatment (14, 28). Rat cortical bone is therefore capable of secondary Haversian remodeling, but it only occurs as an appropriate response to the needs of the bone for repair or for calcium mobilization. In these studies, the extreme nature of the loading applied nearly to the point of overt fracture required an intracortical response. Haversian remodeling in response to overload-induced damage to the matrix of long bone cortex has been reported previously in both dog and rat (1, 5, 29). Mori et al. (29) demonstrated that cortical microcracking in dogs led to an increased intracortical resorptive response, which they interpreted as a programmed renewal of damaged bone. Verborgt et al. (44) showed in a somewhat similar rat experimental system that microdamage colocalized with osteocyte apoptosis, but their studies did not determine whether osteocyte apoptosis preceded the induction of tunneling-type resorption by intracortical osteoclasts. Our data have now demonstrated that it does.

The induction of apoptosis by hyperphysiological strain as well as disuse suggests a possible causative pathway linking cell death and regulation of bone modeling/remodeling. What makes this possible mechanism more interesting is the sequential increase at 7 days but disappearance by 14 days of apoptotic osteocytes, when the first signs of Haversian remodeling were seen. The use of different techniques to establish whether cells were apoptotic or dead (nick end-labeling of DNA, DNA laddering, and LDH activity) provides clear evidence here that very large numbers of osteocytes became apoptotic; moreover, the present evidence suggests that many of these cells had completed their death cycle 7 days later. In none of the sections taken at 7 days, when evidence of apoptosis was clear, were any Haversian canals seen in any sections from any animals. This finding establishes clearly that the osteocyte apoptosis could not be a consequence but might be on the causative pathway leading to intracortical remodeling of damaged bone matrix.

*Cellular Mechanisms*

The magnitude of the osteocyte apoptosis response at 7 days was noteworthy. Unlike necrotic cells, which show early membrane rupture and death (43), apoptotic cells maintain membrane integrity and remain viable during the early stages of cell apoptosis (48). The appearance, 7 days after loading, of DNA damage in osteocytes in loaded bones (as demonstrated by nick end-labeling and DNA laddering) while osteocyte LDH activity remained high is important evidence in support of an apoptotic route to death in these cells. By 14 days, the number of cells with DNA damage was reduced, but the number of nonviable cells had increased proportionately. This suggests that load-induced DNA damage is followed by subsequent events characteristic of the apoptotic process, resulting in nondisruptive cell death within 14 days of the initial damage stimulus. In previous work we found preservation of clearly apoptotic osteocytes within their lacunae, suggesting that the time course of osteocyte apoptosis is longer than that of most other cells types (31, 41).

The absence of increased osteocyte apoptosis in undamaged cortex shown by Verborgt et al. (44) makes it unlikely that overload-induced microdamage can affect osteocyte viability from outside the cell's anatomical territory. It is possible that osteocytes have the intrinsic ability to distinguish pathologically high loading events and to translate their effect into a stimulus to initiate cell death. Stretch-induced apoptosis of cells has, in the case of the myocyte, been shown to involve angiotensin II release and p53 activation (24). The means by which mechanical events are transduced in osteocytes is still unknown but have been suggested to involve direct deformation of the cells or fluid shear (3). The high levels of loading we applied would certainly have increased both these stimuli. Alternatively, matrix microdamage might induce apoptosis by interference with the transmission of strains at a very local level so that the cells close to damaged areas experience very low strains due to isolation from the general strain environment of the bone (35). RGD peptides released adjacent to osteoblastic cells may cause apoptotic cell death (33). It is also possible that cracks in the matrix rupture the cell membranes of osteocyte den-

dritic processes, leading to cytoplasmic leakage and death. Mechanical unloading in genetically modified p53(−/−) animals was associated with preserved bone formation and trabecular bone mass (37), but it is not yet known whether the effects of microdamage on intracortical remodeling require intact p53-p21 signaling.

This study has limitations. The calculations of the mechanical strain levels experienced by individual cells are inevitably approximate as has been discussed elsewhere (30). The neutral axis, is so-called only because it is unaffected by bending (tension-compression); it experiences some strain due to torsion and only approximates the plane of minimum bending load during normal locomotion. Because we cannot study osteocyte apoptosis noninvasively and there is great anatomical variability within the cortex in both osteocyte apoptosis and subsequent intracortical remodeling, it is not possible to conclude that all Haversian remodeling is regulated or even preceded by osteocyte apoptosis.

Because other types of apoptotic cell can induce their own removal by the action of phagocytic cells and also influence the gene expression and cytokine production of neighboring cells (38), it is tempting to speculate that a similar mechanism in bone would account for the programmed direction of osteoclasts to areas of damage and osteocyte apoptosis. Alternatively, such proresorption molecules might in principle also be produced by the resident osteoblast and lining cell population with access to the bone vascular sinusoids (the source of newly arriving osteoclasts) upon encountering osteocyte-derived apoptotic bodies. The nature of any positive or negative chemotactic stimuli to osteoclasts associated with osteocytes requires further investigation. In vitro, bone slices with or without osteocytes are equally well resorbed when osteoclasts are placed on them (19). These data suggest that while osteocytes might directly or indirectly regulate osteoclasts' access or affinity to regions of bone, their presence or absence does not impact on resorptive activity after their arrival. Conversely, antiresorptive extracts and proteins have been produced both from homogenized osteocytes (26) and the osteocyte-like MLOY4 cell line (11), so loss of antiresorption molecules upon osteocyte death might explain the increased resorption we observed in recently damaged bone. In vivo work has demonstrated that transplanted bone previously denuded of osteocytes can undergo reduced, rather than increased, resorption (16) and, also, that regions of osteonecrotic bone are poorly resorbed in vivo (18). These data raise questions concerning the persistence of expression of any signal arising from dying osteocytes that may promote resorption.

In conclusion, in the rat ulna low levels of strain are associated with apoptosis in osteocytes, which can be inhibited by the application of physiological levels of strain. Damagingly high levels of strain also induce apoptosis and subsequent Haversian remodeling. Therefore, there appears to be a J- or U-shaped relationship between mechanical strain and osteocyte survival in the system studied. During these overloading studies, Haversian remodeling never preceded apoptosis but always followed it. We conclude that osteocyte apoptosis is an important candidate mechanism for the precise targeting of osteoclasts to bone programmed to be removed or replaced. It might be fundamental to the successful expansion of the skeleton during growth as well as to some forms of osteoporosis, such as those occurring on abrupt estrogen withdrawal (41).

We thank Prof. John Currey and Dr. Nigel Loveridge for valuable comments on earlier versions of the manuscript.

This work was supported by Medical Research Council Program Grant G9321536 (to J. Reeve) and Wellcome Trust Program Grant 038324/2/96/L (to L. E. Lanyon). J. R. Mosley was funded by a Wellcome Trust Veterinary Research Fellowship. A. C. Brabbs was funded by a White Rose studentship.

Present address of H. Y. Stevens: Tissue Engineering Science Laboratory, 6405 EBU1, Dept. of Bioengineering, Univ. of California, San Diego, 9500 Gilman Dr., La Jolla, CA 92093-0412.

Present address of J. R. Mosley: Royal (Dick) School of Veterinary Studies, Univ. of Edinburgh, Easter Bush Veterinary Centre, Easter Bush, Roslin EH25 9RG, UK.

Present address of G. C. Reilly: Biochemistry Department, School of Dental Medicine, 4001 Spruce St., Philadelphia, PA 19104-6003.

Present address of T. M. Skerry: Dept. of Veterinary Basic Science, Royal Veterinary College, Royal College Street, London NW1 0TU, UK.

## REFERENCES

1. **Bentolila V, Boyce TM, Fyhrie DP, Drumb R, Skerry TM, and Schaffler MB.** Intracortical remodeling in adult rat long bones after fatigue loading. *Bone* 23: 275–281, 1998.
2. **Bronckers A, Goei W, Luo G, Karsenty G, D'Souza R, Lyaruu D, and Burger E.** DNA fragmentation during bone formation in neonatal rodents assessed by transferase-mediated end labeling. *J Bone Miner Res* 11: 1281–1291, 1996.
3. **Burger E, Klein-Nulend J, van der Plas A, and Nijweide P.** Function of osteocytes in bone—their role in mechanotransduction. *J Nutr* 125, *Suppl* 7:2020S–2023S, 1995.
4. **Burger EH and Klein-Nulend J.** Mechanotransduction in bone—role of the lacuno-canalicular network. *FASEB J* 13, *Suppl*: S101–S112, 1999
5. **Burr D, Forwood M, Fyhrie D, Martin R, Schaffler M, and Turner C.** Bone microdamage and skeletal fragility in osteoporotic and stress fractures. *J Bone Miner Res* 12: 6–15, 1997.
6. **Chen C, Mrksich M, Huang S, Whitesides G, and Ingber D.** Geometric control of cell life and death. *Science* 276: 1425–1428, 1997.
7. **Dimmeler S, Assmus B, Hermann C, Haendeler J, and Zeiher AM.** Fluid shear stress stimulates phosphorylation of Akt in human endothelial cells: involvement in suppression of apoptosis. *Circ Res* 83: 334–341, 1998.
8. **Frost HM.** From Wolff's law to the mechanostat: a new "face" of physiology. *J Orthop Sci* 3: 282–286, 1998.
9. **Gross T, Edwards J, McLeod K, and Rubin C.** Strain gradients correlate with sites of periosteal bone formation. *J Bone Miner Res* 12: 982–994, 1997.
10. **Gross TS, Akeno N, Clemens TL, Komarova S, Srinivasan S, Weimer DA, and Mayorov S.** Osteocytes upregulate HIF1alpha in response to acute disuse and oxygen deprivation. *J Appl Physiol* 90: 2514–2519, 2001.
11. **Heino TJ, Hentunen TA, and Vaananen HK.** Osteocytes inhibit osteoclastic bone resorption through transforming growth factor-beta: enhancement by estrogen. *J Cell Biochem* 85: 185–187, 2002.
12. **Hermann C, Zeiher AM, and Dimmeler S.** Shear stress inhibits $H_2O_2$-induced apoptosis of human endothelial cells by modulation of the glutathione redox cycle and nitric oxide synthase. *Arterioscler Thromb Vasc Biol* 17: 3588–3592, 1997.

13. **Hillam RA and Skerry TM.** Inhibition of bone resorption and stimulation of formation by mechanical loading of the modeling rat ulna in vivo. *J Bone Miner Res* 10: 683–689, 1995.
14. **Jee WSS, Mori S, Li XJ, and Chan S.** Prostaglandin $E_2$ enhances cortical bone mass and activates intracortical bone re-modelling in intact and ovariectomised female rats. *Bone* 11: 253–266, 1990.
15. **Kaiser D, Freyberg MA, and Friedl P.** Lack of hemodynamic forces triggers apoptosis in vascular endothelial cells. *Biochem Biophys Res Commun* 231: 586–590, 1997.
16. **Kamijou T, Nakajima T, and Ozawa H.** Effects of osteocytes on osteoinduction in the autogenous rib graft in the rat mandible. *Bone* 15: 629–637, 1994.
17. **Kawata A and Mikuni-Takagaki Y.** Mechanotransduction in stretched osteocytes—temporal expression of immediate early and other genes. *Biochem Biophys Res Commun* 246: 404–408, 1998.
18. **Kenzora JE, Steele RE, Yosipovitch ZH, and Glimcher MJ.** Experimental osteonecrosis of the femoral head in adult rabbits. *Clin Orthop* 130: 8–47, 1978.
19. **Kingsmill VJ, Boyde A, and Jones SJ.** The resorption of vital and devitalized bone in vitro: significance for bone grafts. *Calcif Tissue Int* 64:252–256, 1999.
20. **Klein-Nulend J, Semeins CM, Ajubi NE, Nijweide PJ, and Burger EH.** Pulsating fluid flow increases nitric oxide (NO) synthesis by osteocytes but not periosteal fibroblasts—correlation with prostaglandin upregulation. *Biochem Biophys Res Commun* 217: 640–648, 1995.
21. **Lanyon LE.** Control of bone architecture by functional load bearing. *J Bone Miner Res* 7, *Suppl* 2: S369–S375, 1992.
22. **Lanyon LE.** Functional strain in bone tissue as an objective, and controlling stimulus for adaptive bone remodelling. *J Biomech* 20: 1083–1093, 1987.
23. **Lean JM, Jagger CJ, Chambers TJ, and Chow JW.** Increased insulin-like growth factor I mRNA expression in rat osteocytes in response to mechanical stimulation. *Am J Physiol Endocrinol Metab* 268: E318–E327, 1995.
24. **Leri A, Claudio PP, Li Q, Wang X, Reiss K, Wang S, Malhotra A, Kajstura J, and Anversa P.** Stretch-mediated release of angiotensin II induces myocyte apoptosis by activating p53 that enhances the local renin-angiotensin system and decreases the Bcl-2-to-Bax protein ratio in the cell. *J Clin Invest* 101: 1326–1342, 1998.
25. **Lozupone E, Nico B, Mancini L, Favia A, Lamanna M, and Cagiano R.** The dynamic of the flow of the interstitial fluid into the osteocyte lacunae and canaliculi of bone cultured in vitro. *Bone* 19, *Suppl* 3: 150S, 1996.
26. **Maejima-Ikeda A, Aoki M, Tsuritani K, Kamioka K, Hiura K, Miyoshi T, Hara H, Takano-Yamamoto T, and Kumegawa M.** Chick osteocyte-derived protein inhibits osteoclastic bone resorption. *Biochem J* 322: 245–250, 1997.
27. **Mason DJ, Hillam RA, and Skerry TM.** Constitutive in vivo mRNA expression by osteocytes of beta-actin, osteocalcin, connexin-43, IGF-I, c-fos and c-jun, but not TNF-alpha or tartrate resistant acid phosphatase. *J Bone Miner Res* 11: 350–357, 1996.
28. **Miller MA, Chin J, Miller SC, and Fox J.** Disparate effects of mild, moderate, and severe secondary hyperparathyroidism on cancellous and cortical bone in rats with chronic renal insufficiency. *Bone* 23: 257–266, 1998.
29. **Mori S and Burr D.** Increased intracortical remodeling following fatigue damage. *Bone* 14: 103–109, 1993.
30. **Mosley JR, March BM, Lynch J, and Lanyon LE.** Strain magnitude related changes in whole bone architecture in growing rats. *Bone* 20: 191–198, 1997.
31. **Noble B, Stevens H, Loveridge N, and Reeve J.** Identification of apoptotic changes in osteocytes in normal and pathological human bone. *Bone* 20: 273–282, 1997.
32. **Noble BS and Reeve J.** Osteocyte function, osteocyte death, and bone fracture resistance. *Mol Cell Endocrinol* 159: 7–13, 2000.
33. **Perlot RL, Shapiro IM, Mansfield K, and Adams C.** Matrix regulation of skeletal cell apoptosis II: role of Arg-Gly-Asp-containing peptides. *J Bone Miner Res* 17: 66–76, 2002.
34. **Pitsillides AA, Rawlinson SCF, Suswillo RFL, Bourrin S, Zaman G, and Lanyon LE.** Mechanical strain-induced NO production by bone cells: a possible role in adaptive bone (re) modeling? *FASEB J* 9: 1614–1622, 1995.
35. **Prendergast P and Huiskes R.** Microdamage and osteocyte-lacuna strain in bone: a microstructural finite element analysis. *J Biomech Eng* 118: 240–246, 1996.
36. **Rawlinson SC, el-Haj AJ, Minter SL, Tavares IA, Bennett A, and Lanyon LE.** Loading-related increases in prostaglandin production in cores of adult canine cancellous bone in vitro: a role for prostacyclin in adaptive bone remodeling? *J Bone Miner Res* 6: 1345–1351, 1991.
37. **Sakai A, Sakata T, Tanaka S, Okazaki R, Kunugita N, Norimura T, and Nakamura T.** Disruption of the p53 gene results in preserved trabecular bone mass and bone formation after mechanical unloading. *J Bone Miner Res* 17: 119–127, 2002.
38. **Savill J.** Phagocytic docking without shocking. *Nature* 392: 442–443, 1998.
39. **Skerry TM, Bitensky L, Chayen J, and Lanyon LE.** Early strain-related changes in enzyme activity in osteocytes following bone loading in vivo. *J Bone Miner Res* 4: 783–788, 1989.
40. **Tomkinson A, Gevers E, Witt JM, Reeve J, and Noble BS.** The role of estrogen in the control of rat osteocyte apoptosis. *J Bone Miner Res* 13: 1243–1250, 1998.
41. **Tomkinson A, Reeve J, Shaw RW, and Noble BS.** The death of osteocytes via apoptosis accompanies estrogen withdrawal in human bone. *J Clin Endocrinol Metab* 82: 3128–3135, 1997.
42. **Torrance AG, Mosley JR, Suswillo RFL, and Lanyon LE.** Noninvasive loading of the rat ulna in vivo induces a strain-related modeling response uncomplicated by trauma or periosteal pressure. *Calcif Tissue Int* 54: 241–247, 1994.
43. **Trump B.** Cell death and the disease process. The role of calcium. In: *Cell Death in Biology and Pathology*, edited by Lockshin IBR. London: Chapman and Hall, 1981, p. 209.
44. **Verborgt O, Gibson GJ, and Schaffler MB.** Loss of osteocyte integrity in association with microdamage and bone remodeling after fatigue in vivo. *J Bone Miner Res* 15: 60–67, 2000.
45. **Weinbaum S, Cowin SC, and Zeng Y.** A model for the excitation of osteocytes by mechanical loading-induced bone fluid shear stresses. *J Biomech* 27: 339–360, 1994.
46. **Wolff J.** *Das Gesetz der Transformation der Knochen*. Berlin: Hirschwald, 1892.
47. **Wong S, Evans R, Needs C, Dunstan R, Hills E, and Garvan J.** The pathogenesis of osteoarthritis of the hip. Evidence for primary osteocyte death. *Clin Orthop* 214: 305–312, 1987.
48. **Wyllie A, Kerr J, and Currie A.** Cell death: the significance of apoptosis. *Int Rev Cytol* 68: 251–306, 1980.
49. **Wyllie AH.** Apoptosis: an overview. *Br Med Bull* 53: 451–465, 1997.